Materials Advances

ROYAL SOCIETY OF CHEMISTRY

PAPER

View Article Online
View Journal | View Issue

Cite this: *Mater. Adv.*, 2025, 6, 5149

Extrusion-based additive manufacturing of complex three-dimensional ultra-lightweight materials using the basidiomycete *Fomes fomentarius*†

Huaiyou Chen, *[a] Bertram Schmidt, [b] Andrew Gennett, [b] Paul H. Kamm, [c] Aleksander Gurlo, [a] Vera Meyer [b] and Ulla Simon *[a]

Fungal mycelium-based materials harness the full potential of lignocellulosic resources in a sustainable way. Additive manufacturing can enhance design flexibility and reduce the use of plastic moulds in producing fungal mycelium-based materials. Here, we explored additive manufacturing of living *Fomes fomentarius* for precise fabrication of fungal mycelium-based materials. Using a 1.6 mm nozzle, we extruded a paste containing living fungal mycelium, rapeseed straw, and sodium alginate into various sizes and shapes. The aerial mycelium (consisting of fungal hyphae that grow away from the substrate surface into the air) formed was manually compressed during growth to maintain the desired shapes. For inactivation, freeze drying was found to maintain the original dimensions and shapes of the printed structures more effectively than convection oven drying. In addition to the printed composite materials, pure three-dimensional fungal mycelium skins could also be produced. Electron scanning microscopy, Fourier transform infrared spectroscopy, X-ray microtomography, hydrophobicity testing, compressive and tensile testing were used to investigate the morphological, physical and mechanical characteristics of the printed structures. Our results demonstrate that living *F. fomentarius* mycelium can be successfully used to manufacture lignocellulose–fungal mycelium-based materials with defined growth and hydrophobicity, which further expands its potential for future application as renewable biomaterials.

Received 3rd April 2025,
Accepted 15th June 2025

DOI: 10.1039/d5ma00320b

rsc.li/materials-advances

Introduction

Agricultural and forestry side streams account for a significant portion of global lignocellulosic biomass and have huge ecological and environmental impact in the absence of effective interventions.[1] Filamentous fungi, a group of multicellular and thus mycelium-forming fungi, can be cultivated in such low-cost residual streams and, whilst forming their mycelial networks, produce pure or composite materials.[2–4] Fungal mycelium-based materials have therefore recently attracted significant attention as sustainable alternatives to animal- or petroleum-based products for a variety of applications, including leather-like materials,[5,6] packaging,[7,8] thermal or acoustic insulation,[9–12] and construction materials.[13] State-of-the-art methods for producing such materials typically begin by utilizing moulding techniques to form composites from a lignocellulosic substrate[14] or by obtaining pure fungal mycelium either from liquid cultivations or from aerial mycelium formed on top of solid-state cultivations.[15]

In recent years, extrusion-based additive manufacturing (AM) has emerged as a promising approach to produce fungal mycelium-based materials. This can be achieved by printing a plastic mould from polylactic acid using fused deposition modelling (also named fused filament fabrication), which is then filled with a lignocellulose–fungal mycelium mixture. An incubation period of 1–4 weeks allows the fungal mycelium to grow around and into the lignocellulosic substrate particles, eventually forming a composite.[16–18] An alternative AM approach harnesses direct ink writing (also called robocasting) to directly extrude a fungal mycelium-based paste that contains living or inactive fungal mycelium to produce objects with a desired shape layer by layer. AM with viable fungal mycelium can be used to generate living composites that show self-healing and self-regenerating capabilities.[19,20] In general, the paste has to be homogenous and has to meet certain rheological requirements

[a] *Technische Universität Berlin, Faculty III Process Sciences, Institute of Materials Science and Technology, Chair of Advanced Ceramic Materials, Berlin, 10623, Germany. E-mail: huaiyou.chen@tu-berlin.de, ulla.simon@ceramics.tu-berlin.de*
[b] *Technische Universität Berlin, Faculty III Process Sciences, Institute of Biotechnology, Chair of Applied and Molecular Microbiology, Berlin, 10623, Germany*
[c] *Helmholtz-Zentrum Berlin für Materialien und Energie, Department Microstructure and Residual Stress Analysis, Process Imaging, Berlin, 14109, Germany*

† Electronic supplementary information (ESI) available. See DOI: https://doi.org/10.1039/d5ma00320b

regarding shear thinning properties and sufficient yield stress, whilst maintaining the viability of the fungal mycelium after extrusion. This can be achieved by the addition of hydrogels as thickening agents (water soluble component or agar) but can also contain lignocellulosic substrates (so called composite hydrogels) to sustain fungal growth after the printing process has been finished. While pure fungal hydrogel pastes lead to higher resolution,[19,21] they become more expensive when upscaled. Fungal composite hydrogel pastes offer sustainable opportunities because they upcycle lignocellulosic side streams. A recent review gave an excellent overview on AM of living fungal mycelium and current applications for fungal composite hydrogels.[22] It can be seen that the current nozzle sizes used for fungal composite hydrogel pastes AM are relatively large (greater than 3 mm),[22–24] which makes it difficult to achieve higher resolution prints. Also, the desired shapes are difficult to maintain due to poor or overactive fungal hyphae growth, as well as deformations and shrinkage caused by the drying process.[22,25]

A typical AM process begins with emerse (solid) or submerse (liquid) pre-cultivation of the fungus of interest to obtain sufficient fungal biomass. Afterwards, the mycelial biomass is mixed with the hydrogel to obtain a paste with an adjusted specific viscosity suitable for AM. A second cultivation step of the freshly printed structures allows outgrowth of fungal mycelium and thus solidification of the objects. The overall production process is terminated by the deactivation of the fungal mycelium, when the products are not used with living cells, typically through drying at higher temperature. Notably, incorporating lignocellulosic substrates into fungal composites results in a reduced or even a negative carbon footprint for fungal mycelium-based composites.[26] A current research line of the fungal AM community aims to understand how to optimize paste composition, printing parameters, and rheological properties to foster mycelial growth and much better rational design of fungal mycelium-based materials. As substrates, hemp shives, bamboo or even old paper are usually tested, whereas thickeners such as xanthan gum,[14,27] sodium alginate,[23] chitosan[28,29] or agar[30] are in the current focus of research. Less understood so far is how to inactivate fungal mycelium without affecting the final printed structure characteristics. Also, new approaches are needed to improve print resolution but also to avoid poor, irregular, or even uncontrolled fungal growth that blurs the final structural object design at the end.

We report here a new generation of an AM-suitable paste composition that contains living fungal mycelium from *Fomes fomentarius*, milled rapeseed straw and sodium alginate, which enables us to print 3D objects at high resolution. This study builds on our previous findings that heat-inactivated mycelium of the filamentous basidiomycete and vital fungus *F. fomentarius* can be successfully harnessed for AM.[31,32] Sodium alginate is chosen as the thickening agent because it is bio-based, biodegradable, can be ionically crosslinked, and has good thickening performance.[23,31] To further develop and refine this process, we investigated the feasibility of using living mycelium of *F. fomentarius* in extrusion-based AM, focusing on key process characteristics including fine-nozzle printability, shape preservation during mycelium growth, and structural integrity retention. We can limit unintended outgrowth of aerial mycelium through repeated compression during cultivation which allows us to preserve the designed object morphology. Our comparison of three different inactivation steps reveals freeze-drying as the optimum method able to preserve the structural object design. Finally, we report here an innovative AM-driven process that produces three-dimensional contoured skins out of pure fungal mycelium.

Materials and methods

Fungal cultivation

F. fomentarius strain PaPF11 was cultivated at 27 ± 2 °C (based on our previous experiments and other studies[33–35]) on agar plates containing malt extract as nutrient source for up to two weeks, followed by submerged shake flask cultivation in malt extract broth on an orbital benchtop shaker (Certomat U, Sartorius, Germany) set to a speed of 130 min^{-1} for another two weeks. To prevent any bacterial contamination, both solid and liquid media each contained 50 μg mL^{-1} ampicillin and streptomycin.[35]

Paste preparation

The obtained fungal biomass was filtered through a stainless tea strainer (Yoassi, China), and the wet biomass was dispersed in deionized water (DIW) at a mass ratio of 1 : 4 (fungal biomass : DIW). The fungal suspension was homogenized using a sterile submersion blender (300 W, Siemens AG, Germany) at which point it was ready to be mixed with rapeseed straw powder. This powder was processed from rapeseed straw (Optistraw, Leuven Futtermittel, Germany), milled using a cutting mill (SM100, Retsch, Germany), then screened using multiple sieves (Piccolo, Mogensen, Germany), until it passed through the final mesh size of 0.63 mm as described earlier.[35] The particle size distribution was characterised using a particle size analyser (LS 13 320 XR, Beckman Coulter, Germany). The powder was then autoclaved at 121 °C for 20 min (VX-150, Systec GmbH, Germany). The rapeseed straw powder was then manually mixed with the fungal mycelium homogenate and sodium alginate ($NaC_6H_9O_7$, high viscosity, Alfa Aesar) in the ratio of 11.0 wt% rapeseed straw powder, 86.5 wt% fungal mycelium homogenate, and 2.5 wt% sodium alginate until a homogeneous consistency was achieved. At this point, the paste was considered ready for printing and transferred into sterile syringes. The paste was either directly used or stored at 4 °C before printing. For comparison, a control paste was prepared that consisted of sodium alginate and fungal homogenate (11.3 wt%: 88.7 wt%) only.

Extrusion-based additive manufacturing

Printing was conducted in a biological safety cabinet (LAMSYSTEMS GmbH, Germany) using a home-adapted Ultimaker 2 Go printer (Ultimaker B.V., Netherlands). Here, the filament extrusion part was replaced by an additive manufactured syringe

holder.[31] A tapered dispensing tip with interior ∅ 1.60 mm (Vieweg, Germany) was attached to the syringe, which was connected to a nitrogen bottle with a 0.2 μm filter to prevent airborne contamination. A small piece of sealing film (Parafilm, Amcor) was used on the printing bed for easier transportation, and the areas that exceeded the print range by about 3 mm were cut off to minimize their impact on fungal growth. Cylinders of 20 mm diameter by 10 mm height and 50% infill were printed as the three-dimensional support system moved, driven by 2 bars of pneumatic pressure. In addition to cylinders, other printed shapes such as cuboids, a pyramid, a snow man, and a bear, the heraldic animal of Berlin were chosen. The freshly printed objects were transferred to Petri dishes with a cap of 1 mL DIW to ensure high air humidity, and sealed with sealing films (Parafilm, Amcor). All samples were incubated under 27 ± 2 °C[33,34] and dark conditions for three weeks to allow the regrowth of *F. fomentarius*. For some printed objects, outgrowth of aerial mycelium was manually compressed at the end of each week to keep their original printed shape. A sterilized stainless-steel spatula was used to apply compression. The movement of the spatula was stopped as soon as a distinct increase in resistance was felt, indicating closeness to the scaffold structure. These samples were named 'compact mycelium composites (CMC)'. After 3 weeks of growth, fungal growth was terminated and fungal biomass was inactivated using three different methods: (i) convection-driven oven drying at 70 °C for 6 h, (ii) convection-driven oven drying at 150 °C for 2 h, and (iii) freeze-drying. The latter involved freezing at −80 °C for 2 h followed by vacuum drying at −50 °C, 0.100 mbar overnight in a FreeZone 2.5 Liter Benchtop Freeze Dryer (Labconco, Kansas City, U.S.). The shrinkage of a sample was calculated by dividing the length or volume reduction after drying by the respective values before drying. In some samples, the aerial mycelium layer was manually peeled off from the surface after drying to obtain three-dimensional shaped pure fungal mycelium skins.

Mechanical testing

Compressive tests and uniaxial tensile tests were conducted for freeze-dried CMC or pure fungal mycelium skin. Five printed mycelium cylinders with designed dimensions (*i.e.*, dimensions right after extrusion) ∅ 20 mm × 10 mm were compressed in a mechanical tester (Kammrath & Weiss GmbH, Dortmund, Germany) with a compressive speed of 20 μm s^{-1}. Tests ended when the load reached 450 N, which was slightly lower than the limits of a built-in load cell (500 N). Uniaxial tensile tests were conducted to investigate the strength of pure aerial mycelium skins obtained from the surface of printed mycelium composites. In total, five specimens (20 mm × 10 mm) were cut from the longer side of three printed mycelium cubes with designed dimension 25 mm × 15 mm × 15 mm. A mechanical tester (Kammrath & Weiss GmbH, Dortmund, Germany) with a 10 mm width at clamping ends and a 500 N load cell was used. The displacement control was in the opposite direction compared to the compressive test but at the same speed of 20 μm s^{-1}. For strain calculation, callipers were used for measuring the dimension of the specimens, including the cross-section area as described earlier.[32,35]

Hydrophobicity testing

Water contact angles were measured to determine the hydrophobicity of the printed objects before and after compaction. Before testing, all samples were freeze-dried and stored in a desiccator. 10 μL of deionized water was gently deposited onto the top surface of the fungal mycelium layer using a 20 μL pipette (Eppendorf) held approximately 1 cm above the surface. The side-view images of the water droplets were taken at the mid-height of the water drop with a Keyence VHX-7000 digital microscope (Keyence Deutschland GmbH, Neu-Isenburg, Germany) 90 s after of deposition. In total, six independent points were measured for each sample series, and the results were presented as mean ± standard deviation. Image analysis was carried out in ImageJ with the plugin Drop Analysis-167 LB-ADSA.[36]

Digital light microscopy

Images were taken from the top, side, and sections of the printed fungal composites and stitched using Keyence VHX-7000 (Keyence Deutschland GmbH, Neu-Isenburg, Germany).

Scanning electron microscopy

Fungal mycelium composites were sputtered at 30 mA with gold for 15 s in a sputter system (Sputter coater 108auto, Cressington, Germany) and subjected to scanning electron microscopy (SEM) as described earlier.[12,35] A Quanta 400 ESEM (FEI, USA) was used, detecting backscattered electrons (BSE) in a low vacuum mode. The SEM images obtained were used to determine the hyphal projected density, which we defined as the complement of the pore area ratio. The latter was calculated by applying a threshold to distinguish the mycelium from the background in the SEM images. Using ImageJ (1.53 K), the upper threshold was set to 65 535 (white), which is also the upper limit of pixel values for a 16-bit image. The lower threshold was set to 13 041 for the same 16-bit image, *i.e.* any pixel with an intensity below this value was excluded from the analysis. A pore area ratio was calculated by determining the proportion of pixels within the threshold range relative to the total area of the image. The hyphal projected density was calculated using the following formula:

$$\text{Hyphal projected density} = 1 - \text{pore area ratio} \quad (1)$$

Microcomputed tomography

A representative freeze-dried ∅ 22 mm × 11 mm cylinder sample was analysed *via* microcomputed tomography (μCT) using a microfocus X-ray source at 80 kV and a CsI flat panel detector (Hamamatsu Photonics K.K, Japan) as described earlier[37] with a magnifying geometry of 5× resulting in an effective pixel size of 10 μm. 2000 projections were acquired with an exposure time of 3 × 1.5 s for each angle. Reconstruction was done with X-Aid (MITOS GmbH, Germany) using the Feldkamp–Davis–Kress (FDK) algorithm and 3d rendering with Dragonfly 3D World (Comet AG, Switzerland).

Results and discussion

Living mycelium of *F. fomentarius* can be printed into complex 3D-shaped composites

To develop an optimum paste composition that allows printing of living mycelium of *F. fomentarius*, we decided to use rapeseed straw as both a nutrient supply and structural component, as we could previously show that the fungus grows well on this lignocellulosic substrate.[35] Sodium alginate was used as a thickening agent, as it performed very well in forming a printable formulation for AM with inactive *F. fomentarius*.[31] Up to 30 mm tall structures with various shapes were extruded using a 1.6 mm nozzle, and the fungal mycelium was alive after extrusion with sufficient nutrients for growing into thick three-dimensional skin on the surface of the supporting scaffold (Fig. 1 and Fig. S1, ESI†). When no rapeseed straw powder was present in the paste, the fungus could only grow a very short period after which growth ceased (likely because of the lack of nutrient supply) and the extruded shape collapsed (Fig. 1a). Another problem with pure alginate hydrogel paste was its high-water volume content, known to induce extra spikes on the surface (Fig. 1a, after drying),[38] although the overall shape was maintained after freeze-drying.

This effect became mitigated when rapeseed straw powder was included in the paste formula. Its presence increased the stability of the extruded filaments and the void volume of the printed structures and allowed ice to form more evenly without destroying the printed object design (Fig. 1). Thus, rapeseed straw powder is a key to provide sufficient nutrients to the fungal mycelium and maintain the stability of the paste.

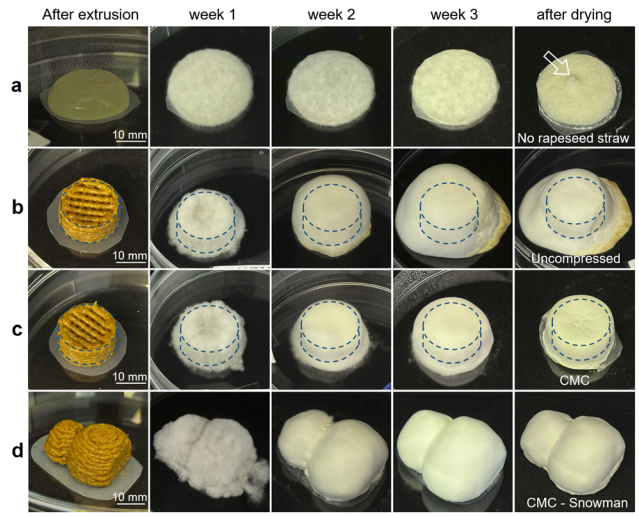

Fig. 1 Images of fungal mycelium growth recorded over three weeks on different extruded pastes, shapes and interference means: (a) rapeseed straw-free paste extruded in a cylindrical shape but deformed, (b)–(d) paste containing rapeseed straw and sodium alginate was extruded in cylindrical or snowman-like form while (b) was incubated without compression and (c) and (d) were compressed at the end of each week of cultivation. The dashed lines in (b) and (c) indicate the contours of the original printed shapes. The pictures were taken before every week's compression. All samples were freeze dried and are shown in the last column.

After 3 weeks of cultivation, fungal mycelium completely covered the surface of the printed shapes and grew into a thick skin-like layer. Due to the generally very expansive nature of radial and aerial growth of filamentous fungi, the printed object morphology changed into a bell shape (Fig. 1b). Notably, the bell shape shows a pronounced outward growth from the bottom of the structure, greater than the height from the top of the structure. The exact driving forces behind such an extensive aerial growth are not known yet, but we speculate that they might be due to carbon dioxide gradients caused by cellular respiration in the closed Petri dish,[39] gravitropism,[40] or other environmental factors. We noticed however, that any uncontrolled expansion of the aerial mycelium could be easily prevented by manually compressing the fungal mycelium. By doing so at the end of each cultivation week, we ensured that the mycelial growth became restricted to the surface of the printed scaffold and were thus able to preserve the desired shapes (Fig. 1c and d). As more complex and even larger object morphologies will be very difficult to be controlled by manual compression, we envision robot arms in the near future that *e.g.* apply compressed air or change locally the cultivation atmosphere or any other conditions to limit unintended growth of the fungus along the supporting plane.

Remarkably, the fungal mycelium remained viable after storing the ready-to-use printing paste at 4 °C for 4 weeks and colonized the printed structures as expected (Fig. S1c, ESI†), which could be interesting from an industrial manufacturing point of view, as it can increase production flexibility and reduce costs in the future.

Freeze-drying preserves printed object morphology

When it comes to using printed fungal mycelium-based materials in everyday life, complete inactivation of fungal growth will likely be required by regulation. However, it is not trivial to preserve the morphology and stability of the printed structural design by drying as such a process usually causes shrinkage of biological matter. Indeed, Fig. 2a shows various shrinkage or deformation phenomena of the manually compacted mycelium objects under different conditions. When drying at 70 °C for 6 h in a convection oven, the average diameter, height, and volume of the cylinders were reduced by 13.7 ± 1.7%, 35.0 ± 2.4%, and 51.6 ± 1.9%, respectively. Also, the dried samples were not only shrunken but also deformed, resulting in volcano-like shapes with a wider lower part, a narrower upper part and a distinct depression in the centre of the upper surface (Fig. 2a). This can be explained by the fact that the viscosity of the sodium alginate gel decreases when the temperature increases;[41] hence it failed to maintain its original shape and started to collapse when there was not enough support. At the same time, the structure of a 50% infill grid pattern enclosed by a continuous wall, coupled with the evaporation of water, resulted in the volcano-like shape by a combination of gravitational and capillary forces. When the drying temperature was increased to 150 °C, the liquification of the alginate gel was even higher, resulted in a higher height shrinkage of 43.3 ± 4.1%, while the shrinkage of diameter and volume were 10.9 ± 3.6% and 54.8 ± 5.9% (Fig. 2a). In addition, in both hot air-drying methods,

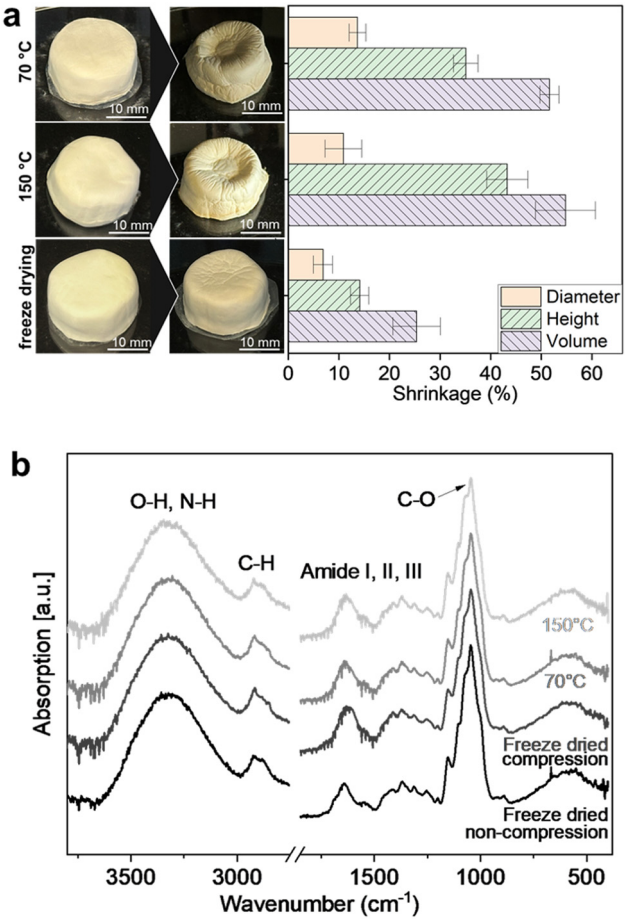

Fig. 2 Effect of different drying methods on the dimensions and chemical composition of mycelium composites from Fig. 1c. (a) Shrinking and deforming on diameter, height, and volume of the printed CMC cylinders after drying in a convection oven at 70 °C or 150 °C, or after freeze-drying. (b) ATR-FTIR spectra for aerial fungal mycelium layer with or without compression during the growth after freeze-drying, as well the compressed layer after drying in a convection oven at different temperatures. The spectra were normalized by 0 to 1.

the colour of the supporting scaffold changed from light brown to dark brown, supposedly because of Maillard reactions of *F. fomentarius*.[12]

Remarkably, the shape of the printed cylinder was very well preserved after freeze drying, with shrinking in diameter, height and volume limited to only 6.8 ± 1.9%, 14.1 ± 1.8%, and 25.4 ± 4.7%, respectively. However, some fine wrinkles appeared on the surface and the increased thickness due to the aerial mycelium made it slightly larger than the designed structure. The final height, diameter, and volume were 11.7 ± 2.4%, 13.3 ± 2.4%, and 43.6 ± 7.9% larger than the design values, respectively. Additional viability tests showed that freeze-drying effectively inactivated the fungal mycelium, whereas brief freezing at −20 °C or −80 °C did not completely eliminate fungal growth (Fig. S2, ESI†).

Attenuated total reflection Fourier transform infrared (ATR-FTIR) spectra of the fungal mycelium cultivated on the printed scaffold methods are shown in Fig. 2b. Independently of manual compression during cultivation and the drying methods after cultivation, all spectra showed similar results in the corresponding absorption bands, *i.e.*, a broad stretching band of O–H and N–H at 3328 cm^{-1}, a stretching vibration band of C–H at 2916 cm^{-1}, an amide I (C═O stretching) band at 1640 cm^{-1}, amide II (N–H bending and C–N stretching) bands at 1556 cm^{-1}, an amide III band around 1373 cm^{-1}, and a strong stretching C–O band at 1046 cm^{-1}. The relative intensities of the absorption bands are very similar to the spectrum of the *F. fomentarius* fruiting body that we observed earlier.[42]

Fig. 3 displays in more detail the changes in 3D morphologies of the printed objects after applying different drying methods that we could observe *via* light microscopy. Drying in a convection oven at 70 °C or 150 °C maintained in general the grid structures of the samples but led to shrinkage of the internal filaments from the designed 1.6 mm to ∼0.5 mm and deformation of the fungal mycelium layers (Fig. 3a and b). In contrast, the structure of the samples remained very well preserved after freeze-drying with respect to both the shape of the individual filaments (∼1.5 mm) and the internal grid layers (Fig. 3c). Compared to the outer surface, the internal volume between the scaffold had only a small number of loose hyphae in all observed samples, resembling pure gel paste printing as reported earlier for the fungus *Ganoderma lucidum*.[19] Additionally, as illustrated in Fig. 3d, the section view of non-compressed composite confirmed the bell shape originated from the extensive radial and aerial growth of fungal mycelium.

Microstructural analyses reveal differences in the three-dimensional architecture of fungal materials

3D-reconstructed μCT images of the manually compacted fungal objects showed that the printed grid structure remained well preserved and thus remained unaffected due to fungal growth (Fig. 4a). Hyphae of *F. fomentarius* have a diameter of about 3 μm and were unfortunately not detectable using the μCT approach used in this study (effective pixel size of 10 μm) but can be detected when higher resolutions are used.[12] However, the microstructural consequences of the drying method could be analysed by the μCT resolution used in this study. Freeze-drying of the compacted mycelium composites resulted in the typical ice-crack pattern, with embedded rapeseed straw fragments. At the bottom-layer cross-section, the external layer of densified hyphae was visible at the structure's periphery. The slight inward collapse of the structure makes the bottom cross-section slightly larger than the top (Fig. 4a).

Scanning electron microscopy (SEM) was used to characterize the internal morphologies of the printed fungal objects. A division between sparse and dense hyphal regions became clearly visible – sparse hyphae connected the dry sodium alginate and rapeseed straw particles, and grew into a dense layer of fungal mycelium in the outer zone (Fig. 4b). A section view of the aerial fungal mycelium layer uncovered that the hyphae in uncompressed sample appeared to be more stretched out (Fig. 4e), while those from manually compacted mycelium composite were more twisted and appeared to be more branched (Fig. 4d). Another noticeable difference between them was the

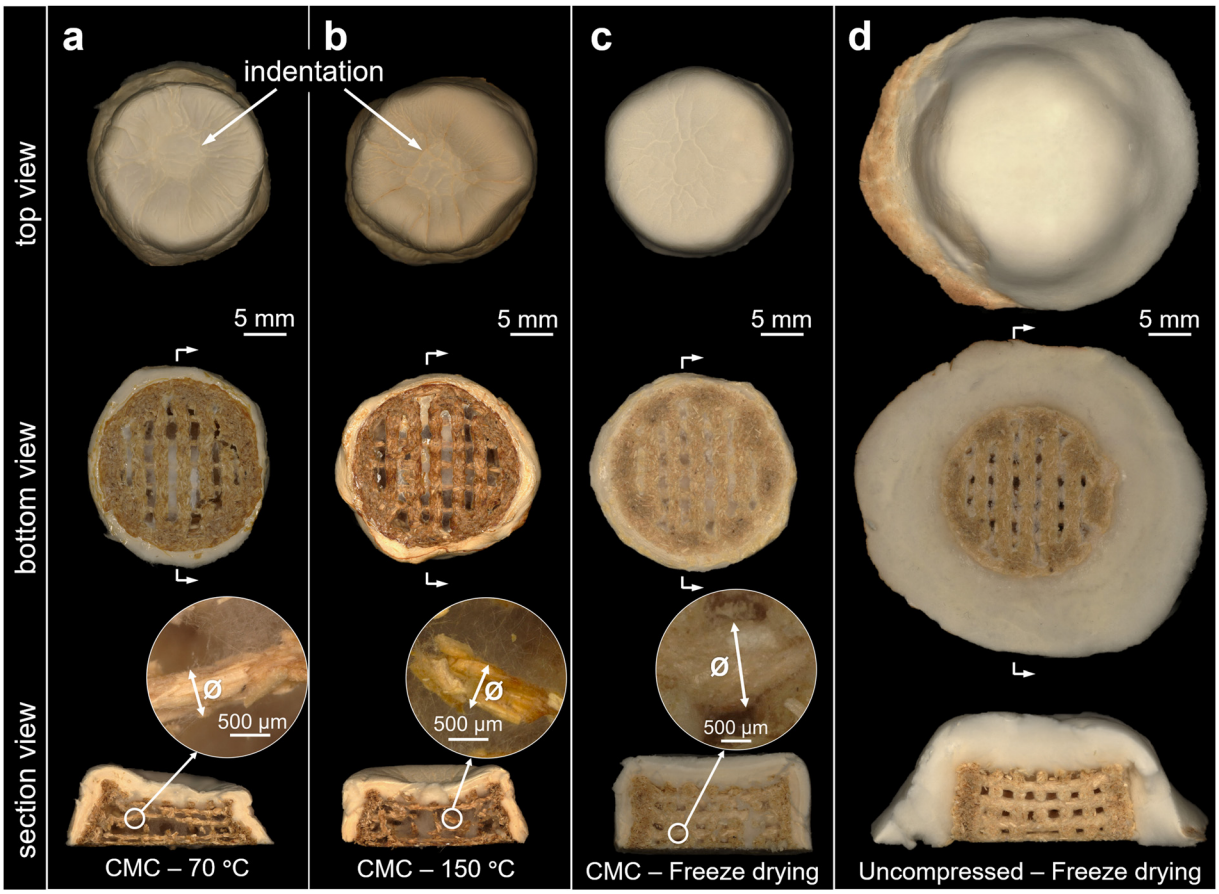

Fig. 3 Morphological images of mycelium composites dried under different conditions. From top to bottom: the top view, bottom view, and section view of the additively manufactured fungal mycelium samples dried in a convection oven at (a) 70 °C, (b) 150 °C, or (c) and (d) freeze-dried. The sample in (d) was naturally grown without other interference while (a)–(c) were compressed during cultivation. The arrows at the bottom view images indicated the viewing direction for the section view. A partially enlarged area was attached in the section view with a separate scale bar.

hyphal projected density. By adjusting the threshold of the pixel intensity in the SEM images, we selected those hyphae that were clearly observed at the same depth (see the Materials and methods section) and uncovered that the hyphal projected density in CMC was higher than the uncompressed mycelium samples (~89% *versus* ~76% at ×2000 magnification, Fig. 4d and e) (more results at different magnifications can be found in Fig. S3, ESI†). This suggested that manual compression does not have a significant inhibitory effect on fungal growth; rather, it resulted only in a denser mycelial network. The higher projected density may be associated with more curled and branching structures as well (Fig. 4e), which might be related to the cellular response of the fungus to the mechanical stress applied.

The printed fungal objects are ultra-lightweight and water-repellent

Several tests were performed to gain deeper insights into the physical characteristics of the printed and manually compacted fungal composites. Most intriguingly, a bulk density of ~0.06 g cm^{-3} of the ∅ 22 mm × 11 mm cylinder made the object light enough to be carried by the stigmas of a *Helleborus niger* flower (Fig. 5a), which demonstrated its lightweight property. We also noticed that it was very easy to peel off the compacted surface from the printed objects in their entirety, so that completely intact three-dimensional shaped fungal mycelium skin was obtained (Fig. 5b and Fig. 6c). This, remarkably, opens new avenues of manufacturing complex shapes of mycelial mats, whereby 3D-printed fungal mycelium shapes or moulds serve as carriers or substrate beds for the designed shapes. The presence of sodium alginate anchored the lignocellulosic particles in the scaffold very well, making for a clean peel without excess substrate material attached. We therefore printed and cultivated several other and more complex shapes for AM of *F. fomentarius*, all of which resulted in well-designed objects including a 10 mm × 10 mm × 10 mm pyramid (Fig. 5c), a ∅ 20 mm column up to 30 mm in height (Fig. S1a, ESI†), and an 83 mm × 50 mm × 10 mm Berlin bear (Fig. S1b, ESI†).

As it is well known that the water resistance of fungal mycelium-based composites is mainly dependent on the cell surface composition of fungal mycelia,[43,44] we tested the water-related properties of composites obtained with *F. fomentarius*. Indeed, the printed objects were able to float on water, demonstrating a hydrophobic behaviour of the composites (Fig. 5d).

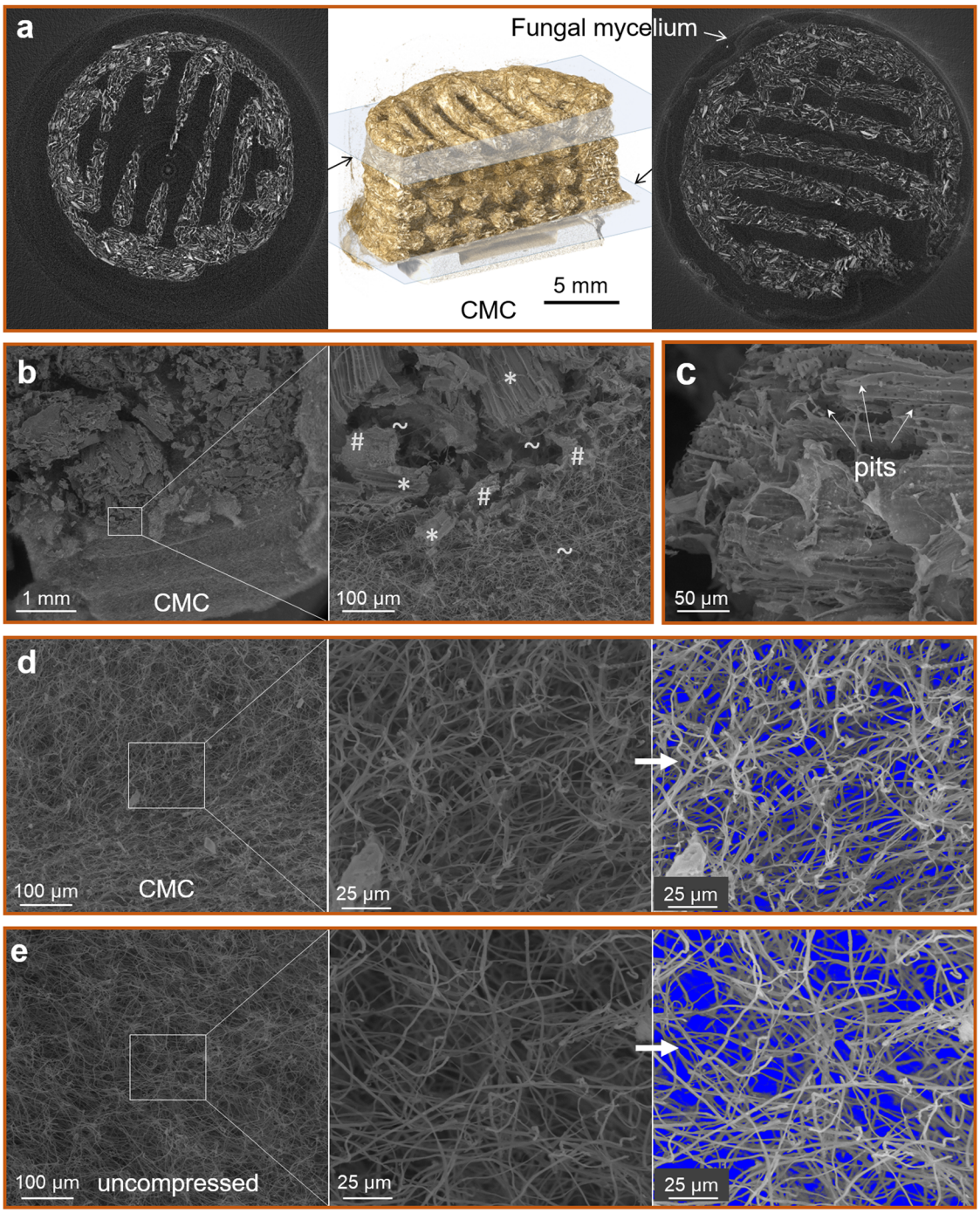

Fig. 4 Microstructure and tomographic imaging of the printed mycelium composites. (a) 3D reconstruction of X-ray microtomography images (middle) of the CMC, and the 2D slices from the top layer of printed scaffold (left) or the bottom layer (right). In the 2D images, white regions represent the solid components of rapeseed straw powder and sodium alginate, while black regions indicate voids or materials with low X-ray attenuation including hyphae. Scanning electron microscopy images of (b) the cross-section of a compacted mycelium composite and an enlarged view at the fungal mycelium skin-printed scaffold border. For clarification, three representative location of each of the major components were labelled, with fungal mycelium by a tilde (~), sodium alginate by a pound sign (#), and rapeseed straw powder by an asterisk (*); (c) a fragment of rapeseed straw being partially wrapped by sodium alginate, (d) the cross-section of the pure fungal mycelium from a non-compressed composite at ×500 and ×2000 magnifications, and the image of the latter after adjusting the thresholds, and (e) the cross-section of the pure fungal mycelium from a CMC at ×500 and ×2000 magnifications, and the image of the latter after adjusting the thresholds.

Notably, the manual compression during cultivation did not prevent or significantly alter hydrophobic properties. In contrast, the aerial mycelium surface on CMC showed water contact angle of 150.32 ± 7.03° (Fig. 5e), which was higher than that of uncompressed aerial mycelium (136.42 ± 9.81°, Fig. 5f) after 90 s of water drop deposition. We note, however, that the

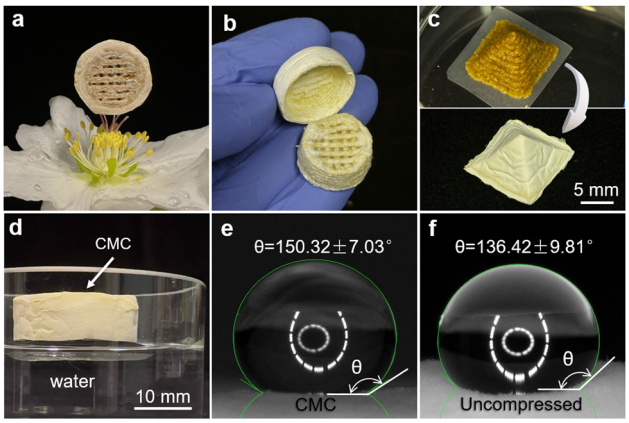

Fig. 5 The ultra-lightweight compact mycelium composite and three-dimensional pure mycelium skin can be made into different shapes and kept hydrophobic. (a) A super lightweight CMC (∅ 22 mm × 11 mm, 0.25 g) was held up by the stigmas of a *Helleborus niger* flower. (b) The aerial mycelium layer being peeled off from a CMC without destroying its 3D shape. (c) A CMC in the shape of a 10 mm × 10 mm × 10 mm pyramid just printed and freeze-dried after three weeks of growth. (d) A ∅ 22 mm × 11 mm cylinder floated on the surface of distilled water with mycelium-covered side in contact with water. (e) and (f) water contact angles of 10 μL of distilled water deposited on the surface of the fungal mycelium layer with (e) or without (f) compression during the cultivation. The pictures were taken 90 s after placing the water drop. Representative samples are shown here.

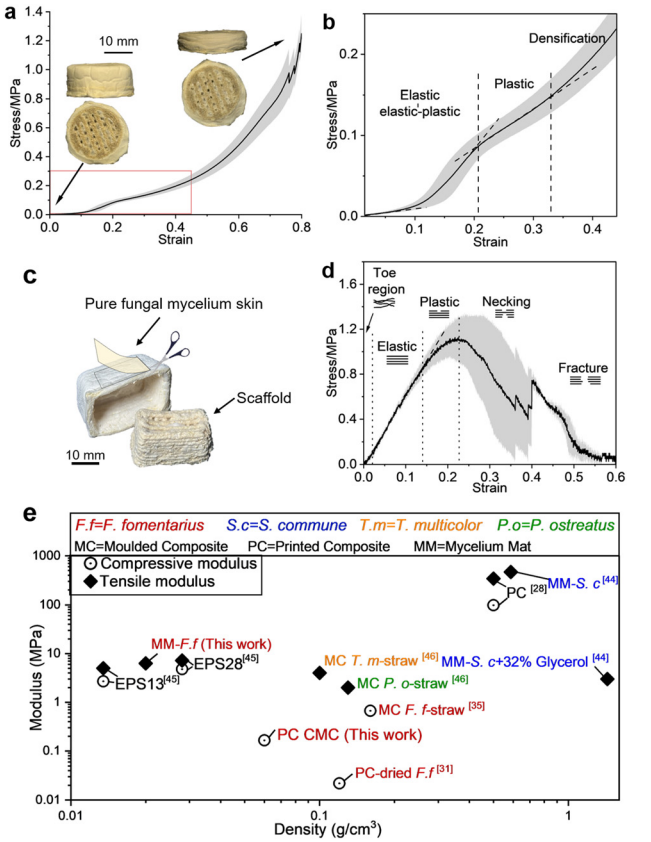

Fig. 6 Compression testing of the compact mycelium composites and tensile testing of the pure mycelium skin. (a) Mean stress–strain curve of the compressive test on printed fungal mycelium composites (n = 5), where the side view and bottom view of a representative specimen before and after the compression are shown, (b) an enlarged view of (a) in the strain range 0–0.45; (c) a schematic diagram of the pure fungal mycelium tensile testing sample obtained from the surface of a CMC cuboid, (d) the mean stress–strain curve of the tensile test of pure fungal mycelium sheet (n = 5) with the schematics of the straightening and failure of the hyphae. (e) The compressive modulus of CMC is compared with that of EPS foams at different densities,[45] moulded *F. fomentarius*-rapeseed straw foams,[35] and other printed composite.[28] The tensile modulus of pure fungal mycelium skin/mat obtained in this work is compared with that of EPS foams[45] and other fungal mycelium-based composites, including plasticizer-treated mats[46] and printed composites.[28,44]

water contact angles were not precisely measured microscopically as the water droplets created indentations on the surface of aerial mycelium, thus making the droplets appear to be embedded. The aerial mycelium appeared to be fluffier and softer on uncompressed surface, thus making it easier to trap water droplets, further reducing its hydrophobicity.

The printed fungal objects show elastic-plastic behaviours

We finally performed several mechanical tests to determine the elasticity and tensile strength of the 3D printed objects. In compressive testing of CMC cylinders, the stress–strain curve underwent three phases (Fig. 6a and b): at low deformation, the pure fungal mycelium layer was compressed in a relatively linear elastic manner. As the deformation increased, the slope of the curve also increased, indicating the onset of deformation of the printed scaffold and an increase in stiffness of the composite material as compared to the pure fungal mycelium layer. Compared to *e.g.*, expanded polystyrene foam (EPS) with a density of 13.5 kg m^{-3}, which has a compressive stress of 0.089 MPa at 10% strain,[45] our printed sample exhibited a lower compressive stress of 0.013 ± 0.006 MPa at 10%, primarily due to the soft fungal mycelium layer on the top. In the second phase, the slope of the curve decreased due to the onset of plastic deformation and microstructural changes. In the third phase, the slope of the curve increased again, reflecting the densification of the composite until the load reached the limit of the load cell. Having reached the limit of compression to 20%–30% of their original height, the samples were permanently deformed. Remarkably, the structure of the printed bottom layer remained intact, with the now compressed debris confined by the bottom layer and the pure fungal mycelium layer (Fig. 6a). At 50% compression, the CMC was able to resist a compressive stress of 0.30 ± 0.04 MPa, which is similar to the value for rapeseed straw-fungal mycelium composites from *F. fomentarius* obtained by moulding, even though the sizes of the lignocellulosic particles are different (Fig. 6e and Fig. S4, ESI†).[35]

For uniaxial tensile testing, we used pure fungal mycelium skins peeled from manually compacted mycelium composites (Fig. 6c). In the beginning, we observed a toe region up to ~2% strain (Fig. 6d) and the slope of the stress–strain curve was nonlinearly increasing with loading. Based on the spatial arrangement and hyphal morphology seen under SEM (Fig. 4d), this was probably due to the straightening of the wave-like

hyphae. After the hyphae were completely straightened, an elastic region started, where the stress and strain were linearly related to a mean elastic modulus $E = 6.31 \pm 1.24$ MPa.

With increased stress, plastic deformation began and the hyphae underwent destructive changes until reaching an ultimate tensile strength at 1.16 ± 0.30 MPa, which is slightly higher than that for cold-pressed *F. fomentarius* mat obtained from static liquid cultivation (0.65 ± 0.2 MPa).[32] Following this plastic region, a long necking region appeared, possibly due to the loose arrangement of hyphae which enabled them to rearrange and slip. Hyphae were thus gradually moving towards their final fracture in a process of constant restructuring and fragmentation. Note that the mean cure in Fig. 6d was calculated from five curves with different strains for the final fracture point, which leads to the fluctuations in the final stage of the curve. Compared with the *Schizophyllum commune* fungal mycelium film produced from liquid shaken cultures with added 32% glycerol (E = 3 MPa and ultimate tensile strength 1.8 MPa),[46] the fungal mycelium sheet obtained in this study has a similar ultimate tensile strength but is stiffer (Fig. 6e).

Conclusions

In this study, we used material extrusion-based additive manufacturing to convert rapeseed straw powders into sustainable fungal mycelium composites and pure fungal mycelium skin. Various shapes (*e.g.*, cylinders, pyramids, snowman, bear, *etc.*) with heights up to 30 mm were manufactured using a 1.6 mm print nozzle. After three weeks of cultivation, the growth of fungal mycelium in each printed object was successfully restricted to its predefined shape using manual compression and thus prevented uncontrolled expansion during cultivation. Freeze-drying performed better than other fungal inactivation methods such as convection oven drying and minimizing shrinkage while retaining both the outer shapes and internal structures of the printed objects. After drying, the three-dimensional skin made of pure fungal mycelium could be peeled off from the printed scaffold, resulting in structures with complex shapes, optimized tensile strength, and high elasticity. Rather than using the fungal paste immediately after preparation, it can be stored at 4 °C for at least 4 weeks, eliminating the need for repeated paste preparation, which could potentially optimize efficiency of the overall process. Finally, we have shown here that AM of fungal mycelia opens more sustainable avenues as previously anticipated, *e.g.* for application of fungal mycelium-based materials in packaging, filtration, acoustic insulators, biodegradable structural components, soft materials, *etc.* On the one hand, it can replace plastic moulds often employed in traditional production schemes of fungal mycelium-based composites. On the other, the ability to produce complex three-dimensional fungal mycelium structures, both in their composite and pure mycelium variants, unlocks new opportunities for the application of fungal mycelium materials in other fields.

Author contributions

H. C.: conceptualization, methodology, investigation, data curation, visualization, writing of the original draft, writing – review & editing; B. S.: conceptualization, methodology, supervision, project administration, writing – review & editing; A. Ge.: methodology, investigation, writing – review & editing; P. H. K.: methodology, investigation, writing – review & editing; A. Gu.: resources, supervision, project administration, writing – review & editing; V. M.: resources, supervision, project administration, writing – review & editing; U. S.: conceptualization, methodology, supervision, project administration, writing – review & editing.

Conflicts of interest

There are no conflicts to declare.

Data availability

The data supporting this article have been included as part of the ESI.† Any additional data required for replication or further inquiry can be obtained upon request.

Acknowledgements

The authors would like to thank Carsten Freidank-Pohl, Annika Thoma and Isabel Regeler (Chair of Applied and Molecular Microbiology, TU Berlin, Germany) for support in fungal mycelium preparation and viability testing, Stefan Platzk (Chair of Mechanical Process Engineering, TU Berlin, Germany) for milling the rapeseed straw, Claudia Fleck and Sophie Klemm (Chair of Materials Science & Engineering, TU Berlin, Germany) for support in mechanical testing, Michelle Schumann (Chair of Materials Science & Engineering, TU Berlin, Germany) for help in SEM measurements, and Francisco Garcia-Moreno (Department Microstructure and Residual Stress Analysis, Process Imaging, HZB, Germany) for help in μCT analyses. Open Access funding was enabled and organized by Projekt DEAL.

Notes and references

1 C. Cabeza, J. Gaffey, K. Hendriks, N. Hatvani, E. Lambrecht and H. Welck, *Potential of biomass sidestreams for a sustainable biobased economy: Bringing added value to agriculture and forest sectors by closing the research and innovation divide*, Steinbeis-Edition, Stuttgart, 2019.
2 N. Attias, O. Danai, T. Abitbol, E. Tarazi, N. Ezov, I. Pereman and Y. J. Grobman, *J. Cleaner Prod.*, 2020, **246**, 119037.
3 J. K. Muiruri, J. C. Chuan Yeo, Q. Zhu, E. Ye, X. J. Loh and Z. Li, *ACS Sustainable Chem. Eng.*, 2023, **11**, 6801–6821.
4 P. Gough, A. Globa and D. I. E. Reinhardt, in*Sustainability and Toxicity of Building Materials*, ed. E. K. Petrović, M. Gjerde, F. Chicca and G. Marriage, Woodhead Publishing, 2024, pp. 547–571.

5 M. Jones, A. Gandia, S. John and A. Bismarck, *Nat. Sustainable*, 2021, **4**, 9–16.
6 MycoWorks - Growing the Future of Materials with Fine Mycelium™, **https://www.mycoworks.com/**, (accessed January 15, 2025).
7 K. Joshi, M. K. Meher and K. M. Poluri, *ACS Appl. Bio Mater.*, 2020, **3**, 1884–1892.
8 Mushroom Packaging, **https://mushroompackaging.com/**, (accessed January 15, 2025).
9 muvobit, Acoustic, **https://mogu.bio/acoustic-collection/**, (accessed January 15, 2025).
10 K. B. Bonga, L. Bertolacci, M. Contardi, U. C. Paul, M. S. Zafar, G. Mancini, L. Marini, L. Ceseracciu, D. Fragouli and A. Athanassiou, *Macromol. Mater. Eng.*, 2024, **309**, 2300449.
11 M. G. Pelletier, G. A. Holt, J. D. Wanjura, L. Greetham, G. McIntyre, E. Bayer and J. Kaplan-Bie, *Ind. Crops Prod.*, 2019, **139**, 111533.
12 B. Schmidt, C. Freidank-Pohl, J. Zillessen, L. Stelzer, T. N. Guitar, C. Lühr, H. Müller, F. Zhang, J. U. Hammel, H. Briesen, S. Jung, H.-J. Gusovius and V. Meyer, *Fungal Biol. Biotechnol.*, 2023, **10**, 22.
13 M. Jones, A. Mautner, S. Luenco, A. Bismarck and S. John, *Mater. Des.*, 2020, **187**, 108397.
14 E. Elsacker, S. Vandelook, A. Van Wylick, J. Ruytinx, L. De Laet and E. Peeters, *Sci. Total Environ.*, 2020, **725**, 138431.
15 L. M. Henning, U. Simon, A. Abdullayev, B. Schmidt, C. Pohl, T. Nunez Guitar, C. Vakifahmetoglu, V. Meyer, M. F. Bekheet and A. Gurlo, *ACS Omega*, 2022, **7**, 4158–4169.
16 N. Alima, *Res. Dir.: Biotechnol. Des.*, 2024, **2**, e18.
17 MY-CO BUILD | Futurium, **https://futurium.de/en/my-co-build**, (accessed January 15, 2025).
18 E. Klarenbeek, Eric Klarenbeek's Mycelium Chair, **https://www.ericklarenbeek.com/**, (accessed January 15, 2025).
19 S. Gantenbein, E. Colucci, J. Käch, E. Trachsel, F. B. Coulter, P. A. Rühs, K. Masania and A. R. Studart, *Nat. Mater.*, 2023, **22**, 128–134.
20 S. Schyck, P. Marchese, M. Amani, M. Ablonczy, L. Spoelstra, M. Jones, Y. Bathaei, A. Bismarck and K. Masania, *Global Challenges*, 2024, **8**, 2400104.
21 C. Reyes, E. Fivaz, Z. Sajó, A. Schneider, G. Siqueira, J. Ribera, A. Poulin, F. W. M. R. Schwarze and G. Nyström, *ACS Sustainable Chem. Eng.*, 2024, **12**, 16001–16011.
22 A. Mohseni, F. R. Vieira, J. A. Pecchia and B. Gürsoy, *Biomimetics*, 2023, **8**, 257.
23 A. M. Rahman, Y. M. Akib, C. O. Bedsole, Z. Pei, B. D. Shaw, C. O. Ufodike and E. Castell-Perez, *Biomimetics*, 2024, **9**, 411.
24 E. Elsacker, E. Peeters and L. De Laet, *Sustain. Futures*, 2022, **4**, 100085.
25 A. Bhardwaj, A. M. Rahman, X. Wei, Z. Pei, D. Truong, M. Lucht and N. Zou, *J. Manuf. Mater. Process.*, 2021, **5**, 112.
26 A. Livne, H. A. B. Wösten, D. Pearlmutter and E. Gal, *ACS Sustainable Chem. Eng.*, 2022, **10**, 12099–12106.
27 H. Li, S. Xie, S. Cao, L. Hu, D. Xu, J. Zhang, H. Mo and Z. Liu, *Foods*, 2022, **11**, 1443.
28 S. C. Shen, N. A. Lee, W. J. Lockett, A. D. Acuil, H. B. Gazdus, B. N. Spitzer and M. J. Buehler, *Mater. Horiz.*, 2024, **11**, 1689–1703.
29 E. Soh, Z. Y. Chew, N. Saeidi, A. Javadian, D. Hebel and H. Le Ferrand, *Mater. Des.*, 2020, **195**, 109058.
30 E. Soh, J. H. Teoh, B. Leong, T. Xing and H. Le Ferrand, *Mater. Des.*, 2023, **236**, 112481.
31 H. Chen, A. Abdullayev, M. F. Bekheet, B. Schmidt, I. Regler, C. Pohl, C. Vakifahmetoglu, M. Czasny, P. H. Kamm, V. Meyer, A. Gurlo and U. Simon, *Fungal Biol. Biotechnol.*, 2021, **8**, 21.
32 H. Chen, S. Klemm, A. G. Dönitz, Y. Ou, B. Schmidt, C. Fleck, U. Simon and C. Völlmecke, *ACS Omega*, 2024, **9**(50), 49609–49617.
33 U. Peintner, R. Kuhnert-Finkernagel, V. Wille, F. Biasioli, A. Shiryaev and C. Perini, *IMA Fungus*, 2019, **10**, 17.
34 P. Dresch, M. N. D'Aguanno, K. Rosam, U. Grienke, J. M. Rollinger and U. Peintner, *AMB Express*, 2015, **5**, 4.
35 C. Pohl, B. Schmidt, T. Nunez Guitar, S. Klemm, H.-J. Gusovius, S. Platzk, H. Kruggel-Emden, A. Klunker, C. Völlmecke, C. Fleck and V. Meyer, *Fungal Biol. Biotechnol.*, 2022, **9**, 4.
36 A. F. Stalder, T. Melchior, M. Müller, D. Sage, T. Blu and M. Unser, *Colloids Surf., A*, 2010, **364**, 72–81.
37 L. Liu, P. Kamm, F. García-Moreno, J. Banhart and D. Pasini, *J. Mech. Phys. Solids*, 2017, **107**, 160–184.
38 K. G. Libbrecht and K. Lui, *J. Glaciol.*, 2004, **50**, 371–374.
39 United States, US20150033620A1, 2015.
40 D. Moore, *New Phytol.*, 1991, **117**, 3–23.
41 A. S. Finny, N. Cheng, O. Popoola and S. Andreescu, *Environ. Sci.: Adv.*, 2022, **1**, 443–455.
42 S. Klemm, C. Freidank-Pohl, L. Bauer, I. Mantouvalou, U. Simon and C. Fleck, *PLoS One*, 2024, **19**, e0304614.
43 M. B. Linder, G. R. Szilvay, T. Nakari-Setälä and M. E. Penttilä, *FEMS Microbiol. Rev.*, 2005, **29**, 877–896.
44 F. V. W. Appels, S. Camere, M. Montalti, E. Karana, K. M. B. Jansen, J. Dijksterhuis, P. Krijgsheld and H. A. B. Wösten, *Mater. Des.*, 2019, **161**, 64–71.
45 W. Chen, H. Hao, D. Hughes, Y. Shi, J. Cui and Z.-X. Li, *Mater. Des.*, 2015, **69**, 170–180.
46 F. V. W. Appels, J. G. van den Brandhof, J. Dijksterhuis, G. W. de Kort and H. A. B. Wösten, *Commun. Biol.*, 2020, **3**, 1–5.